NEW FUEL CELL TUBULAR ARCHITECTURE AND THE EFFECT OF ELECTROKINETIC FLOWS IN ITS PERFORMANCE

Luis Antônio Waack Bambace, bambace@dem.inpe.br
Alfredo José Alvim de Castro, ajcastro@ipen.br
Instituto Nacional de Pesquisas Espaciais-INPE. Av. Astronautas 1758. São José dos Campos. CEP 12201-970
Instituto de Pesquisas Energéticas e Nucleares. IPEN Av. Prof. Lineu Prestes, n.2242 São Paulo CEP 05508-000

Abstract. This paper describes a new fuel cell electrodes architecture family based in porous walls tubes obtained with mm-nonwoven fabrics templates. With use of: proper impregnation of anodes tubes walls; mm-scale flange systems and eventual thin covers of hydrogen permeable metals in anode tubes, cross flow is eliminated without membranes. Fabrics insulate electrodes. Electrokinetic flows improve ionic transport and cells take advantage from high breathing areas to increase reactants supply and drop chemical polarization. All the processes needed to build these set ups exists, but need improvement to reach the required quality level for reliable prototypes building. Cell gas flow is alike a car air filter one. To raise the chances of success, many alternative options were studied to each cell part or process. Concept working, building techniques, performance and technical risks are also studied.

Keywords: fuel cell, nanometer metal foams, carbon nanotubes, H_2 filtering shell, transportation.

1. INTRODUCTION

Low temperature fuel cells have more free energy, but have slower catalysis and worse transport phenomena limitations. Catalysts need reactants, electrical and ionic current drain. A dry platinum grain on a carbon black particle has full access to gas reactants, but any ionic current drain without contact with the ionomer, by other hand a like grain totally covered with ionomer has a very difficult or inexistent access to reactants. In flooded catalysis zone all catalyst has ionic transport, but the access to reactants limited by gas diffusion in water. In most painted type Membranes Electrode Assembly, MEA, it is not possible to know if the catalysis occurs in mist, totally dry or all flooded media, as their theoretical performance is too close. This is shown in the data of Roshandela et al. (2005), Sunet al. (2005), Thampan et al. (2001), Antoineet al. (2001) and Al-Baghdadi (2005). Anode catalyst CO poisoning is other problem, if it is exposed to ppm of it at temperatures below 403 K. Electroosmose pumps anode H_2O to the cathode in Proton Exchange Membrane cells, PEM, so the thicker the membrane the harder to keep anodes hydrated with cathode produced H_2O. Painted MEA also have big electrical resistance due to a difficult electron transfer among carbon grains. The diffuser gas flow drag causes only low speed gas flow in dry catalyst, with big O_2 concentration changes in air operation. Many solutions tried to solve such problems, as catalyst on ordered arrays of carbon nm-fibers normal to membranes (Chang et al. 2007), air chicanes (Sunet al. 2005), gas flow mm radius-tubes placed in liquid electrolyte (Tennison, S.R. and Sowerby 2003), carbon fiber fabrics electrodes with Entangled Carbon Nanotubes, ECN, covers (Ledoux et al. 2004), microfluidics set ups (Ramos et al. 2008). Initially, we bet in a single material and membrane use, with breathing area maximization as main goal, to get low polarization wholly wet catalysis, trying to increase O_2 transport by convection. Later, we saw the importance convective ionic current, that many higher porosity tube wall materials with were available, and as O_2/H_2 diffusion grew convection lost meaning. Finally we saw that proper anode wall impregnation and catalyst location would easy cross flow and poisoning control, while reducing ionomer losses.

2. CELL SET UP AND PRODUCTION PROCESSES.

The basic dirty H_2 cell set up is "Fig. 1" to "Fig. 5". Cathode tubes have uniform catalyst load in its porous walls.
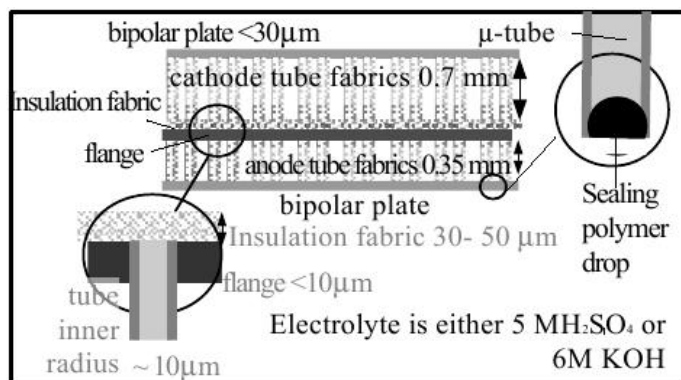

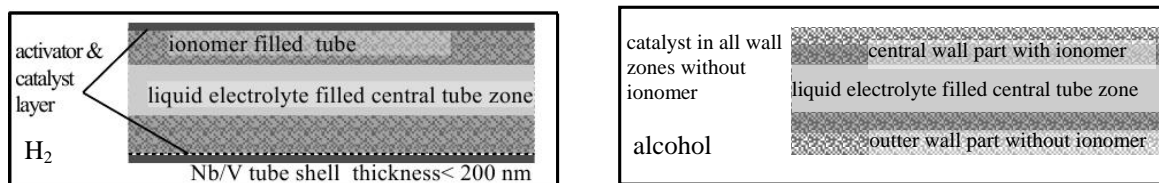Figure 1. Typical cell lateral cross section

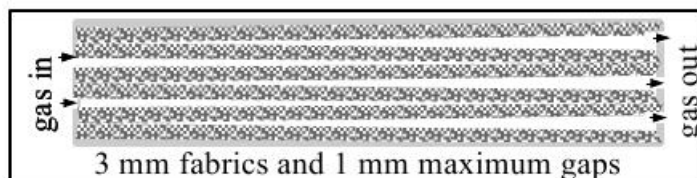Figure 2. H$_2$ and alcohol anode tubes cross sections

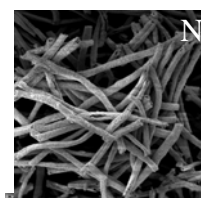Figure 3. Anode & cathode top view with gas flow scheme

Figure 4. SEM Images of Nano Structured Metal Foam, NSF, 5 μm inner radius & 70-100 nm foam cell elements
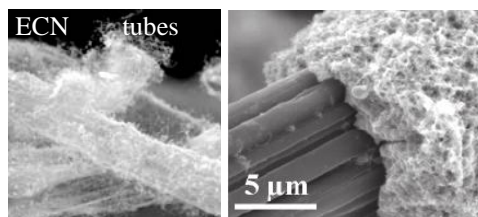

Figure 5. SEM Images of tubes of Entangled Carbon Nanotubes walls (ECN), and Ledoux ECN covered carbon fiber

Direct NSF electroplating, with surfactant intermediation is one path to get proper tube walls. Despite this process is described in the literature as a potential problem to electroplating leveling, (Vermilyea, 1957), nickel NSF was first introduced in (Bambace et al. 2007). Plating in high specific area items requires care with gas trapping, reactants transport and fibers vibration, that strongly differs from a material to another. Radiolytic chromium deposition in Ni-NSF, followed by hot Cr diffusion, and 1200°C nitriding, assures tube walls of inert material, chemically equal the Los Alamos laboratory bipolar plated material obtained by nitriding directly plated NiCr alloys (Brady et al. 2004). A description of radiolytic process for catalysts deposition is in (Silva et al. 2005), and this process is used to apply metal catalyst over tubes impregnation layer. As surface tension is the energy needed to form an unit area of a specific interface, if the gelling volume of a polymer solvent solution that wets a porous walls set is exactly this set volume, it will fill only these walls, in order to minimize total surface energy, if it is smaller, only the tubes central zone will be filled. Melting and solidifying slowly the polymer reduces porosity. Nickel boride layers building over the NSF is also an alternative protection way. Direct building of NSF with NiCr alloys showed itself too difficult and expensive. ECN tubes were also made. Using carbon fibers as growing substrate it is not possible to remove it without destroying ECN. Luckily partially burned material, metal and alumina microfiber fabrics are also good substrates to ECN growing. Metal and some partially burned materials allow diffusion of catalyst, reducing the nm-tubes quantity to a given catalyst amount. Different work gases needs different temperatures, and metal cannot be used with all gases. The adopted techniques where the ones of Ledoux et al. (2005) and Antunes et al. (2006). Many metals that in past required hot fused salt electroplating may now be plated at room temperature with ionic liquids as imidazolium chloride, amides and organic sulfur compounds. More, Nb was one of the first metals deposited with its chlorides, imidazolium chloride, and AlCl$_3$ as optional compound to better ionic conductivity (Cheek et al. 1999). After testing this patent protected process, we seek another path; in special we used a bath of VCl$_3$ and CH$_3$-H$_2$S-CH$_3$, C2H$_5$-H$_2$S-C$_2$H$_5$ euthetic mix. Fabric surface impregnation with metal chlorides raises the growing rate of metal in the direction parallel to the support surface, as well as it reduces porosity. If gelling volume of ionomer is exactly the one of the tube sets porous wall, and surface energy of

solid is lower than solvent ionomer surface tension, it fills near exactly wall pores, if smaller only central part of porous walls. Gelling of H_2 impermeable polymer solution drops at tubes tips, seals it, and if this is done before filtering metal is applied the barrier it is more efficient. But before doing so, it is needed to build the flanges, doing a temporary tip sealing with the same method. Tips sealed, for instance with acrylic, may be pressed towards a tyxothropic mix of polymer, its specific solvent and colloidal silica, or such silica and its preparation suspension emulsions. After cure, a rotating sand paper set up removed excess of polymer and the tip protection is dissolved with specific solvent by ultrasonic cleaning. Possible room temperature cure polymers are high melting temperature PVC, Poly (4-methyl pentene-1) and Poly (vinyl fluoride) among others. Carded fabrics with fiber normal to bipolar plates have the shortest ionic path, but available fabrics are thin, and assembly with many fabrics shall be used. Entangled Poly (acrylonitrile) fabrics with most of the fibers with a low angle with a chosen direction are available for carbon fiber fabrics production, and are thicker and easier to handle. Process cracks effects in cells in an open issue. The main ECN problem is current transfer between nm-tubes that may be raised by building graphite bondings among them, a process in test. The more aligned the nm-tubes are with a line normal to the template fiber axis, harder is the electron drain. This isn't a problem in anodes due to the H_2 permeable V/Nb cover conductivity. Ledoux fabrics may be used in cathodes, if neither ECN nor NSF reach design goals, but ionic resistance will be higher.

3. THEORETICAL BACKGROUND

Static electrocapillary was described by Lippmann in the 19th century, who saw that mercury surface tension had a parabolic profile with a maximum for uncharged liquid. For more complex electrolyte, surface tension σ is given as a function of its value for pure uncharged liquid σ_o, the electrical capacity C, the area A, the electrical potential U, bath to wall potential difference ΔU, influence coefficients B_i, the concentration of dissolved ion i [a_i], and constants b_k by the Grahame Model as:

$$\sigma = \sigma_o - 0.5 \, (C/A) \, \Delta U^2 + \Sigma_i \{B_i \, ln(1 + b_k \, [a_i]) \, \} \qquad (1)$$

The capacity per unit of area c= (C/A) depends on ΔU. The capacitive energy is $c\Delta U^2/2$. As a rule of thumb derivatives of energy with displacements are forces in displacement direction. The surface tension is the energy needed to create a unit of a specific interface area. If only electrical parameters vary with plate parallel position y, cΔU(dU/dy) is the electrocapillary force. Few works (Bambace et al. 2007) showed electrocapillary convection experiments, of flow speeds in cm/s order, see Fig. 6. Filming bubbles generated in the reservoirs connected with triangular channels, one dielectric one metal, the latter contacting asymmetric secondary electrodes, with energized electrodes far away the separation, such flow is observed. To explain the forces an illustrative set up with cathode, anode, fluid and a middle plate is in Fig.7. The plate potential minimizes capacitive energy. Normal field for a single layer of charges is ΔU/δ, total charge cΔU and pressure $c\Delta U^2/\delta$, for δ the distance of the charges to the surface. Pressure acts between charges and surface, so 2cΔU(dU/dy) is the pressure gradient force, as parallel field is dU/dy, the direct electrostatic force is cΔU(dU/dy). There's an uncharged line, not central as adsorption in anode and cathode is unequal. Edge charge concentration is higher. Assuming continuous dielectric and single plane of charges, 3cΔU(dU/dy) is the total force ƒ over a surface element. The apparent paradox is explained by the fact that this force is a system internal one. A 2cΔU(dU/dy) force asides ion to ion direct electrostatic ones opposes Electrical Boundary Layer, EBL, is the internal resistance.
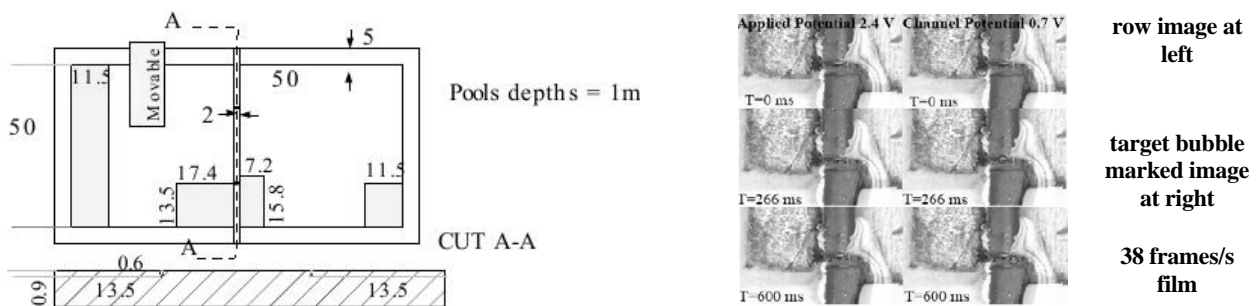

Figure 6. Electrocapillary flow observation set up, and some frames from one of the hundred filmed observations cases
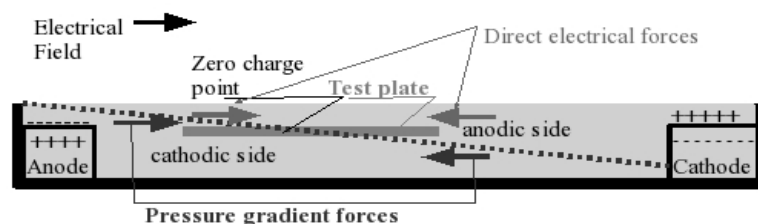

Figure 7. Sketch of electrocapillary forces in a conductive plate placed in an electrolyte with strong current

Continuous dielectric models don't treat exactly ion to ion direct forces. If Grahame model is right, inner dissipation and resistances shall reduce net forces over uncharged fluid just for $c\Delta U(dU/dy)$. Electroosmotic Flow, EOF, differs from electrocapillary one, as chemical equilibrium in EOF causes a constant charge density. Non-solvated ions are ions in contact with metal plates not surrounded by H_2O molecules, even if their charge is contrary the plate ones, discharge doesn't occur if it raises Gibbs free energy. A minimum nucleation radius calculation is based in equilibrium between release of chemical and electrostatic energies and increase in surface energy. The closest place, x_2, of such ions center defines the Inner Helmholtz Plane, IHP. Next is the nearest place of solvated ions centers, the Outside Helmholtz Plane, OHP. Contrary charge ions are pulled to the wall by metal charges, and only if ion to ion repulsion is included big forces repelling ions from the wall appears. The non-diffuse charged layers close attached to the surface is the Stern layer, with many phenomena in it as: Van der Wals forces, dipoles, hydrogen bridges, and surface diffusion. Thermal motion and shocks flip ions in the bath and there is a distribution of charges near the wall, a diffuse EBL sub-layer, dEBL. Only dEBL and Stern layer have charge unbalances. To very high EBL cross potentials, total capacities tends to the Stern layer one, and capacities stop to show dependence with ion concentration. EBL is studied in the Double-Layer theory that uses somehow a charge unbalance distribution (Bizzotto 2002). The Gauss law links total charge inside a control volume and electrical field, it is joined with other hypothesis to get charge profiles. Models as: Normal and Modified Poisson-Boltzmann, PB/PB^M, Poisson-Nernst-Planck, PNP, and Brownian Dynamics Model, BD (Corry et al. 2003), differs in: studying ion sizes and relative potentials, ion diffusion, use of continuous hypothesis and so on. Stern layer dielectric constant is near 30 in OHP, and 6 in IHP. In general, most systems have over 98% of monovalent ions due to ionization constants. PB model uses only a $z_i \varphi$ energy term in a_i distribution, to $\varphi=UF/(R\ T)\equiv \wp U$ and z_i the valence of ith-ion, don't treat ion size neither predict limit surface charge or cathode/anode capacity differences and neglect diffusion, $\ln(\nu_i\ a_i)$, but PNP treats it, spreading dEBL. PB^M adds $Q(x,y)$, a sum of ions relative self energies, with smaller γ_e. PNP exact profiles calls for numerical methods. Poisson equation, to μ_i the chemical potential, ν_i a molar volume, $\tilde{A}(y)$ a best fit constant, gives:

$$\nabla^2\varphi = \Sigma z_i\ a_i\ F = -K^2\ \Sigma n_i\ n_o^{-1} exp(-Q-\mu_i-R\ T\ ln(\nu_i a_i)-z_i\varphi) - (K\ exp(-\tilde{A}))^2\ \Sigma n_i\ n_o^{-1}\ exp(-z_i\varphi) \qquad (2)$$

where potential references are set far away the plate, far ionic concentration is a_∞. T is the absolute temperature, F and R are the Faraday and Universal Gas constants, $K\equiv[2z_i^2 F^2 a_\infty(y)]^{1/2}[\varepsilon R T]^{-1/2}$ is the inverse of the Debyer Length, γ_e the volume charge density, ε the media dielectric constant. $K'=K\ exp(-\tilde{A}/2)$ is a modified Debyer Length. To high ΔU and a_∞, $\tilde{A}$ may reach 10. $\tilde{A}\equiv 0$ in PB. At high dEBL transverse potential, single solvated ion planes give too big γ_e, so N extra solvated ions planes are needed, and the Last Non-diffuse Plane, LNP, is at x_2+x_3. LNP γ_e must be bigger than initial diffuse zone one. If N=0, x_3=0. Implicit form solution of Eq. (2) in is:

$$tanh(0.25\varphi)=tanh(0.25\varphi_2(y))exp(-\underline{K}(x-x_2))\equiv G(x,y) \qquad (3)$$

where $\underline{K}=K\ exp(-\tilde{A})$, $\varphi_2(y)$ is the dimensionless potential at x_2, and x the distance from the plate, to $\varphi/\varphi_2=\xi<<1$, x is the EBL thickness x_*. $\tilde{A}$ fits is better with $N\neq 0$. With $\delta=z\ \wp$ and $\zeta(y)=\varphi_2(y)\delta^{-1}$, explicit form of Eq. (3) is:

$$U(x,y)= 2\ \delta^{-1}\ ln\{1+G(x,y)\} - 2\ \delta^{-1}\ ln\{1-G(x,y)\} \qquad (4)$$

The unit area capacity c has diffuse and non-diffuse parts, c_m and $c_2=\varepsilon/x_2$. $E_o\hat{e}_y+E_x\hat{e}_x$ is the EBL total electrical field $\mathbf{E}$, to $\hat{e}_y$ parallel and $\hat{e}_x$ normal to the metal surface, diffuse charge density ν is $\varepsilon d^2 U/dx^2=4\varepsilon\underline{K}^2\delta^{-1}(G^3+G)(G^4-2G^2+1)^{-1}$. U and ionic resistivity ρ obeys Laplace Equation, so:

$$c^{-1}=c_2^{-1}+c_m^{-1}=x_2/\varepsilon(x_2)+c_m^{-1}=c_2^{-1}+0.5\ x_3/\varepsilon(x_3)+(N+1)^{-1}\varepsilon^{-1}(x)[cosh(\delta\zeta(y)/2)]^{-1}\underline{K}^{-1} \qquad (5)$$

$$\mathbf{E} = -\nabla U \qquad (6)$$

$$\nabla^o(\rho^{-1}\nabla U)= 0 \qquad (7)$$

The Gauss equation is $\gamma_e\sim\varepsilon\ d^2U/dx^2$ for thin EBL. Continuity, Navier-Stokes and species concentration equations are:

$$\nabla^o\mathbf{u} = \nabla^o(u_x\hat{e}_x+u_y\hat{e}_y)=0 \qquad (8)$$

$$\omega\ u_i\ d\mathbf{u}/dx_i = -\nabla P + \mu\nabla^2\mathbf{u} + \gamma_e\ \mathbf{E} \qquad (9)$$

$$-D_i\ \nabla^2 a_i + \mathbf{m_i}\ \nabla^o(\mathbf{E}\ a_i)+ \nabla^o(\mathbf{u}\ a_i) + \chi_{qi}-\chi_{qo} = 0 \qquad (10)$$

where ^{o} means a scalar product, ω is the fluid density, a_i the ith concentration, χ_{qi} and χ_{qo} chemical conversion rates, $\mathbf{m_i}$ ionic mobility, D_i diffusion coefficient, $\mathbf{u}$ fluid velocity. Pressure is $P(x,y)=P_\infty(y)+\varepsilon\ (dU/dx)^2/2$, P_∞ its value out of EBL, as $\mathbf{u}$

components normal to the surface may be neglected in $\mathbf{e_x}$ Navier-Stokes equation for 2nm$<x_o<$5nm if $\zeta(y)\neq0$. Due to adsorbed ions mobility and surface diffusion, plus slipping boundary condition Knudsen numbers, $\mathbf{u}$ may be split in $\mathbf{s}$ normal to wall, equal to zero far the wall, and 4 parallel parts: $u_m= U_m(r^2/R^2)$, $u_p=(\zeta-U)\varepsilon\mathbf{E}_o\mu^{-1}$, an OHP/LNP slip v_{OHP} at x_2, and v_p. $G\equiv0$ out of EBL, dU/dx=0 if U = 0, being the near wall slip, S_w, $v_{OHP}+u_p+v_p$, so:

$$[\varepsilon d^2U/dx^2\mathbf{E}_o-\mu d^2u_p/dx^2]+[dP/dy+4\mu u_mR^{-2}+\Delta P_a+\omega u\,du/dy+\omega\,s\,du/dx]-[\mu d^2v_p/dx^2-\varepsilon dU/dx d^2U/dx dy-\varepsilon dU/dy d^2U/dx^2]=0 \quad (11)$$

Setting each of the bracket terms of Eq. (11) individually to zero, one gets the classical EOF equation, with u_p as solution, an equation that governs the flow out of the EBL, with solution u_m, and a bracket that refers to the electrocapillary extra component v_p, function of electrical variables only. For x-$x_2<x_o$-x_2 and L= 2 d$\underline{K}$(y)/dy = $\underline{K}$ $a_\infty^{-1}da_\infty$/dy:

$$dv_p/dx=\mu^{-1}\varepsilon dU/dy dU/dx \quad (12)$$

$$Y=0.5\,\delta cosech(\delta\,\zeta/2)\,(d\zeta/dy) \quad (13)$$

$$v_p=\delta^2\mu^{-1}\varepsilon\{1-G(x)^2\}^{-1}\{Y-L\,x'\}/2+L\underline{K}^{-1}\delta^2\mu^{-1}\varepsilon ln\{(1+G)(1-G)\}/4+L\delta^2\mu^{-1}\varepsilon x'/2 \quad (14)$$

In narrow gaps a_i and a_∞ vary due to dissociation changes that overcome non-reacting ions migration. PB^M has Q(y) effect in d$\underline{K}$/dy. In 2D cases with a fixed wall potential U_w, the total EBL cross potential ϕ_w is U_w-U, at ϕ_w=0, and also $d\phi_w$/dy=($\underline{K}x_2$+1)dζ/dy, so for linear U profile outside a PB EBL,with $\underline{K}$ definition and Eq.(5):

$$d\phi_w/dy=-0.5\,(U_w-\zeta)\,a_\infty^{-1}da_\infty/dy-0.5\,\delta U_w[tanh(\delta\,\zeta/2)]^{-1}d\zeta/dy+0.5\,\delta\zeta\,tanh(\delta\,\zeta/2)d\zeta/dy \quad (15)$$

Higher dEBL potentials mean bigger $\underline{K}$, due to Q(y), but N has an uncertain effect, as ion sizes and self potentials limit surface charge densities. The near wall effects of the bulk neutral zone flow is negligible, and electrostatic forces are extremely high, so S_w depends on electrical issues only, so it is possible to use the continuity equation to get the traverse velocity components in the EBL, so:

$$dS_w(x,y)/dy + ds(x,y)/dx = d(v_p(x,y)+u_p(x,y)+v_{OHP}(y))/dy+ ds(x,y)/dx = 0 \quad (16)$$

At surface, s is zero if there isn't reaction, or related to a local source or sink reaction term $s_o(y)$. For B=$\varepsilon\mathbf{E}_o\mu^{-1}$, A=B$\zeta$ and M=tanh($\delta\zeta$/4)$^{-1}$ it holds to:

$$s(x',y)=\int_o^{x'(y)}\{-d\,v_{OHP}(y)/dy\,-d\,u_p(x,y)/dy-dv_p(x,y)/dy\}dx\,+s_o(y) \quad (17)$$

$$\Lambda(x,y)=\int_o^{x'(y)}u_p(x,y)dx=x'B\zeta(y)-4\,B\,x'\,\delta^1\,ln(G(x',y)^2)-4\,x'^2\,B\,\underline{K}(y)\,\delta^1 \quad (18)$$

$$\Xi(x,y)=\int_o^{x'(y)}v_p(x,y)dx=\delta^2\mu^{-1}\varepsilon x'\{Y-Lx'\}/2+\underline{K}^{-1}\delta^2\mu^{-1}\varepsilon ln(1-G(x',y)^2)\{Y-Lx'\}/4+0.5\underline{K}^{-1}\delta^2\mu^{-1}\varepsilon ln(G(x',y)^{-2}-1)Lx' \quad (19)$$

The integral of $\gamma_e(\mathbf{u}^o\hat{\mathbf{e}}_y)$ in the EBL planes normal to $\hat{\mathbf{e}}_y$ is the flow current i_F, and it includes Stern layer slips. Items with large EBL transverse potential and big specific areas have big i_F, reducing dU/dy changes to a given current $i_T=i_F+i_m$, with i_m the migration current. Reaction rates, Ω, depends on EBL transverse potential, and di_T/dy=H(y)Ω, for H(y) a geometry factor. For high specific area systems, of free transverse area A_t, iterative schemes shall be used to find the flow current and the coefficients of potential profiles interpolation, as dU/dy=$\rho i_m A_t^{-1}$. The EBL thickness derivative $x'_*(y)$ is easily found. The normal to the boundary layer has a slope is $x'_*(y)^{-1}$, $\{1+x'_*(y)^2\}^{-1/2}$ and $\{1+x'_*(y)^{-2}\}^{-1/2}$ are its normal components, respectively normal and parallel to the plate, the boundary element length is $\{1+x'_*(y)^2\}^{0.5}$dy, as electrolyte bulk is neutral, then the momentum exchange at the EBL-bulk interface shall agree with Eq. (1) values, so using Eq. (8), for $S_{BL}(y)=S_w(x_{d*}(y),y)$:

$$x_{d*}(y)=-ln(tgh(0.25\,\delta\,\xi\,U_2(y)/z)/tgh(0.25\,\delta\,U_2(y)/z))/\underline{K}(y) \quad (20)$$

$$cU(y)dU(y)/dy=-\omega[s_o(y)-x_{d*}(y)dv_{OHP}(y)/dy - d\Lambda(x_{d*},y)/dy-d\Xi(x_{d*},y)/dy]S_{BL}(y) \quad (21)$$

Once given U(y), the $U_2(y)$, $x_*(y)$, $\Lambda(x_{d*},y)$, $\Xi(x_{d*},y)$ quantities and $x'_*(y)$ are known, and $s_o(y)$ may be calculated with reaction rates, equation (21) is in fact an ordinary differential equation to OHP slips as function of position y, also i_T direction. When U(y) and electrolyte concentrations are high the u_p, v_p, and all y derivatives of its x integrals are small face to v_{OHP}, simplifying it, $\omega x'_{d*}(y)S_{BL}(y)^2$ and $\omega x'_{d*}(y)v_{OHP}(y)V_{bounslip}(y)$ are opposite in sign and cancels if $S_{BL}(y)\equiv v_{OHP}(y)$, so:

$$c\ U(y)\ dU(y)/dy = -\ \omega\ [s_o(y) - x_{d*}(y)\ dv_{OHP}(y)/dy]v_{OHP}(y) \tag{22}$$

The interesting in Eq. (22) is that if there is no chemical reaction and diffuse layer effect is negligible, $c_m\ U^2/2$ low, v_{OHP} is proportional to U in the Fig. 7 system. In an analogy with thermocapillary (Dadzie and Méolans, 2005), v_{OHP} has a slip boundary condition part, $(2-\alpha)\alpha^{-1}\mu^{-1}\lambda f$, to α an accommodation coefficient and λ the mean free path, near 0.3 nm to H_2O at 25^oC; and a slip, $hcUdU/dy$, to h a constant, due to surface diffusion, viscosity, and creep the first affected by electrical fields (Swartzentruber 1996). Stern Layer details are in (Bennett 2006). Unlike electroosmose IHP may slip at speed v_{IHP}, mainly due to creep and surface diffusion, typical $\mu^{-1}\lambda f$ is 0.05 to 0.1 mm/s. Flow current integrals were done numerically and depends on v_{IHP}, and charge profiles. Stern Layer slips profile is parabolic. At cell tube ends $i_T=0$, but $U\neq0$, so an integration constant is needed. If surface charging is low i_F is low, but quite big in high charged zones limiting available potentials to the electrokinetic flow and its speeds, even if symmetry kills macroscopic flows. Theoretical 5M H_2SO_4 and gold flat surface Stern-PB model capacitances is near $1\,F/m^2$, but measures over 180 F/m^2 may be found to parts that look polished with naked eye, due to area differences. Electrochemical cells local surface reaction rate currents, j, are linked to local overpotential η, with z_i the total number of moles of charges involved, α accommodation coefficient, i_o the exchange current, D_{eff} the effective diffusion coefficient, [a_o] and [a] the reference and local activities, $\eta=RT\ln\{j[a_o][a]^{-1}i_o^{-1}\}/(z_iF\alpha)$. Diffusion pore electrode [a] varies and for flat systems (Mitchel, 1963) gives for a very long pore:

$$\eta = 2\ R\ T\ ln\{j^2[a_o]^{-1}\ z_{i*}^{-1}\ F^{-1}\ D_{eff}^{-1}\ i_o^{-1}\ \kappa^{-1}\}/(z_i\ F\ \alpha) \tag{23}$$

Where z_{i*}' is the number of charges transferred in a reaction step, and κ is its area per unit of volume. D_{eff} takes in account convective mix, tortuosity, τ, and void fraction, f. Without convection $D_{eff}=D\ f\ \tau^{-1}$. The main electrodes scales q are so small that D/q is in the cm/s range. The bulk flow is laminar, except in few Bénard cells limits of small effect in transport. Transverse speeds near elements are quite low, so only the flux at sharp Nanometer Scale Foams, NSF, edges contributes in the porous zone to enhance radial diffusion transport. But as EBL are thin peak points have 30% increase effect in apparent diffusion coefficient for absolute flat surfaces, representing a 10% mean increase that will be neglected for safety. A 2nd reason to neglect reactants convective transport is that in ECN μ-tubes fabrics flow departure is not modeled. But the main reason to disregard reactant transport is the fact that if capacitance is bigger than predicted charge transport is even better, but convective speeds smaller, reducing importance of convection to mass transport. In any case, decrease in ionic resistance will be greater than flat surface theoretical values, unless conductive surfaces are insulated from electrolyte by contamination.

Breathing surface and catalyst support areas are two important items to the system. A set of tubes of single diameter d and lengths l_i has an volume equal to $(\Sigma l_i)\pi d^2/4$, and a fabric of such tubes of area S, thickness h and void fraction f, has a tube volume equal to $Sh(1-f)$. As the tubes total area is $(\Sigma l_i)\pi d$, the area per unit of fabric area is just $4(1-f)h/d$. For filter mounting a 2nd void fraction is needed, the apparent inter fabrics void fraction f_2, and to an electrode height h_2, the tube area divided by the bipolar plate support area is $4(1-f)(1-f_2)h_2/d$. For nanotubes of diameter d_n catalyst support area ratio is $4(1-f)(1-f_2)(1-f_3)h_2/d_n$ where f_3 is a void fraction of the μm-tubes that considers its central zone and space between nm-tubes. For a foam with area per unit of volume ϖ and tube walls internal and external diameters d_i and d_e the catalyst support area ratio τ is $(1-f)(1-f_2)\varpi h_2\ (d_i/d_e)^2$. For catalyst only in the inner face of the metal filtering shell of diameter d_{is}, the catalyst support area to electrode support area ratio is $4(1-f)(1-f_2)h_2d_{is}\ /d^2$. Notice that every area per unit of volume is a form factor $\Im$, in the 2-6 range in most cases, divided by a characteristic dimension x. To the NSF, x is $7\cdot10^{-8}$ m and $\Im$ near 3.7. So ϖ is about $5\cdot10^7$ m^{-1}. Near the breathing surfaces, catalysts are plenty of reactants, in the inner part of tubes not, if reactivity is high Eq. (23) may be used, if not and the geometry is cylindrical, given exchange current i_o, and activity in its measurement [a_{ref}], and the activity change differential equation to $r_{min}<r_{max}$ zone is the Bessel equation:

$$D_{eff}\ d^2[a]/dr^2 + D_{eff}r^{-1}d[a]/dr =\ \varpi\ i_o[a_o]\ [a_{ref}]^{-1}F^{-1}z_i^{-1}exp(\alpha\ \eta z_i'\ F\ R^{-1}T^{-1}) \tag{24}$$

The right side term doesn't depend on r, but η decreases if farer is a point from a fabric insulator. To $\vartheta=I_1(mr_{min})K_1(m\ r_{min})^{-1}$ and $[a^*]=[a_o]\ [I_0(m\ r_{max})+\vartheta K_0(m\ r_{max})]^{-1}$, solution of Eq. (24) to no O_2 flux at r_{min}, is $[a(r)]=[a^*]\{\ I_0(mr)+\vartheta K_0(mr)\}$, where m is $\{\varpi i_o[a_o]\ [a_{ref}]^{-1}(D_{eff}F\ z_i)^{-1}exp(\alpha\eta z_i'F\ R^{-1}T^{-1})\}^{0.5}$; the current, j_t, per unit of tube wall area is given by $D_{eff}\ F\ z_i\ m\ d[a(r)]/dr$. $2\pi r\ j_t$ is the ionic current exchanged per length of tube, hereafter ι_t. As in a tube $dU/dy=\rho\ i_m$, and $i_T=i_f+i_m$, η may be obtained as function of the distance from fabric insulator. The tubes don't have fixed current as PEM membranes do, they may be not normal to this insulator, where the whole current is ionic, and as there is a void fraction, average near interface current density increases by a factor $(1-f)^{-1}sec^2(\theta_{av})$ where θ_{av} is an average angle to the normal. Hydro entangled fabrics used as carbon fiber precursor may assure $\theta_{av}<30^o$, if its peak resistance direction is normal to insulation. To hydro entangled fabrics with base plane parallel to insulator $\theta_{av}\sim55^o$. The Kirchhoff law says that potential difference between two points doesn't depends on path in a system with many parallel / serial elements. So to a given electrochemical potential, U_{ch}, net potential U_{nch} is fixed, and the sum of losses $U_L = U_{ch}+U_{nch}$, equals to the sum of: EBL transverse potentials; fabric insulators losses $Ui=j\ th_I\ \rho_{eff}$, to th_I its thickness and r_{eff} effective resistivity; local overpotentials η, at cathode $\eta_c(y)$, or anode $\eta_a(y)$; accumulated ionic losses in cathode tube $U_{ci}(y)$ or anode tube $U_{ai}(y)$, and accumulated electrical losses in anode tube $U_{ae}(y)$ or cathode tube $U_{ce}(y)$. See that ρ_{eff} is multiplied by a tortuosity-void fraction ratio, for

fabrics with electrolytes ρ_{eff} is 50 to 100 times smaller than Nafion membranes one. The whole current crosses a fabric insulator or a PEM membrane, the smaller the electrodes texture, the closer j is to the homogeneous one. The total is the current sum of all parallel path currents. Electrodes potentials minimize the free energy to a given current. Near insulation $U_{ai}(y)/U_{ci}(y)$ is smaller, but $(\eta_c(y)+U_{ce}(y))/(\eta_a(y)+U_{ae}(y))$ bigger, and thus mean U losses must be calculated dividing the total energy loss by the average current. Due to intermediate contact the tubes of a single pore electrode transfer both types of current one to the other. Anode / cathode tubes normal to insulation fabrics will have respectively at least 4 / 8 contacts with other tubes. Variations of the angle θ between tube axis and insulation fabric normal is negligible for carded fibers systems. For entangled fabrics with peak resistance direction parallel to insulation fabric normal, variances of θ are near 10°. It was found that constant reaction rate and overpolarizations tubes, with θ equal θ_{av}, always gave a voltage output smaller than complete model at same current, as too big η means excess reactivity near the insulator, and transport controlled reaction rate. It is interesting to see that the flow current reduces dependence of ionic resistances with θ. For higher local EBL transverse potentials the local ionic resistances are smaller. Despite of higher OHP slip speeds, global flow current is smaller than in previous analogy models (Bambace, 2007) due to smaller capacitances. This model included logarithmic radial ionic resistances in tubes, and concentration resistances in fabric insulators. Analysis is restricted to Pt as catalyst and dirty H_2 cell, with very small Pt loads. Ni, Nb and C resistivity are 6.84, 12.5 and 1375 μΩcm, but from 33 to 100 μΩcm to carbon nm-tubes in axis direction (Xue, 2007), so electrical resistances shall be neglect, except uncovered ECN cases. The anode shell H_2 transport is treated in (Bambace, 2008), and its shown in it that H_2 concentration differences between the 2 shell sides are negligible, as well as CO poisoning is not a problem any more even to high fuel CO levels, and that no O_2 pass through this shell

4 CELLS NUMERICAL SIMULATION RESULTS

The model of section 2 was used to evaluate ECN and NSF acid cells performance with 52.5 μg-Pt/cm^{2} in cathode and 33.75 μg-Pt/cm^{2} in anode to 1bar O_2/H_2 pressure, using as reference area the bipolar plate face geometrical one, figs 8 and 9, with H_2SO_4 5M as electrolyte. The 3rd case was a cell with the same Pt loads and 6M KOH, Fig.10, as expected the cell lost performance due to smaller O_2 solubility in KOH, near 1/6 of pure water one, against 4/5 of pure H_2O one to H_2SO_4. The last case is a KOH cell with silver as cathode catalyst, and Pt anode. We designated in the fig. 8 to 11 as clean cells, cells with full theoretical electrokinetic current transport, and as not clean the cells without this current transport. Cells operate with percent CO levels. O_2 are blocked by anode tube shells, and reacts internally with eventual tiny amounts of CO that pass trough shell pores. Change in Tafel slope was not considered.
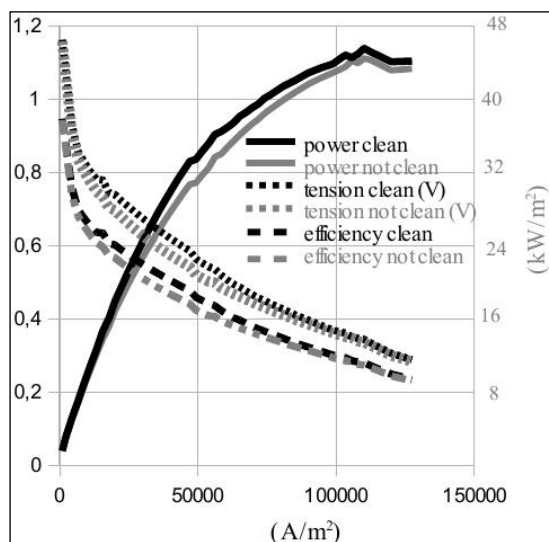

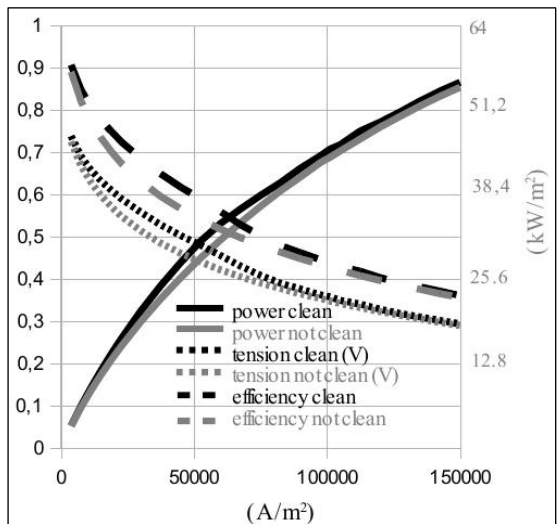Figure 8. Performance of Pt catalyst NSF acid cell

Figure 9. Performance of Pt catalyst ECN acid cell

All cells pack each electrode pair in a 1140 μm space as cathode, anode, protected metal bipolar plate, flange and electrolyte filled fabric have thickness of respectively 700 μm, 350 μm, 30 μm, 10 μm and 50 μm. So it is possible to pack 8.77 electrodes pair each centimeter. The peak power of 4.6 W/cm^2 of the NSF acid cell is multiplied by packing factor is near 40 kW/dm^3, at near 28% efficiency. At 50% efficiency this cell produces 24.5 kW/dm^3. With assumption of standard Carbon conductivity in fig.9 cell, and 30° of average nm-tubes angle to μ-tube axis normal, acid ECN cells reach 48 kW/dm^3 at peak, and at 25.3 kW/dm^3 50% efficiency. If axial nm-tube data is used ECN performance improves a few kW/dm^3. At peak power it is difficult to remove produced heat. As forces over fabrics is proportional to square of flow speeds, higher pressures, as 5 to 10 bar to both H$_2$ and air, means reasonable concentration changes and cooling without high stress in electrode fabrics, 5 bar air and H$_2$ may be used at this condition an improvement in performance is expected. With 5 bar air, 18 m/s speeds will assure less than 20% O$_2$ level change.
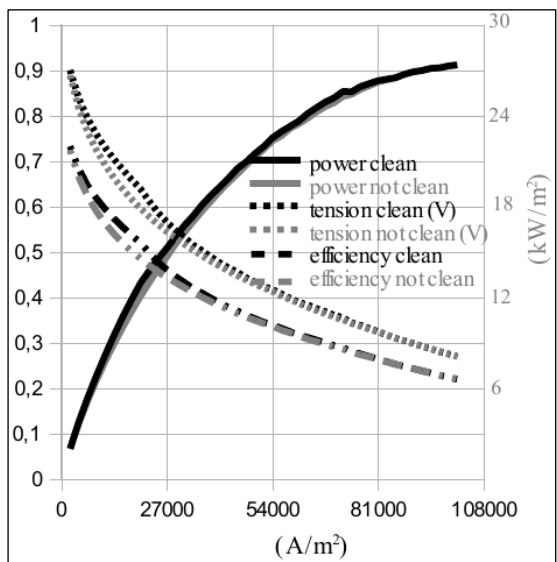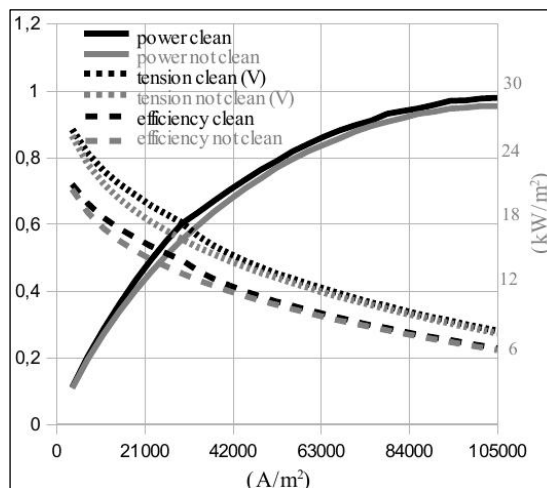

Figure10. Performance of Pt catalyst NSF alkaline cell

Figure11. Performance of Ag/Pt catalyst NSF alkaline cell

It is possible to see that the Ag catalyst performance is even better than Pt one, and the reason for that is the larger catalyst amount used, with alike grains size, once in both cases radiolytic processes are used. In the same way the higher breathing and catalyst support areas favors the use of alkaline and acid spinel catalyst as well as nitrogen pyropolymers with Fe or Co as central metals, if its grain size is compatible to the small dimensions of the substrates. Due to smaller activity these catalysts were not useful to traditional PEM geometries, but usable in tubular ones, as soon as suitable deposition process becomes available. Bacon geometry has an 1/3 void fraction to electrolyte in the fine grain part of the electrode, that roughly occupied 50% of its volume, and in the waved metal part that controlled the gas flux, alternate high and low pressure zones, that promote a near contact zone gas flux only. If all pores were dry, Bacon cell would have 3/7 of present geometry cathode breathing area, true area is less as pores far from gas supply are total or partially flooded. The catalyst support area of Bacon cell was also smaller than, as well as it has less suitable ionic transport geometry. In all dry pores, only 1/6 of void to electrolyte, besides two scales of tortuosity, but due to uncertain flooding, some parts have 2/3 void to it. There was a fine grain total flood 1/3 void to electrolyte layer of 0.05 mm in bacon design. In current design reaction starts with full breathing just close to large electrolyte void fabric separator, where potential available to speed it is maximum. Cathode void to electrolyte is near 35%. Due to that differences performance is better either to Pt as well as to spinel. Non Pt catalysts still have uncertain of bad durability, as Ag, but we hope that with the availability of a suitable design to its use future research turns available a suitable non-Pt catalyst. It shall be noticed that the amounts of Pt per unit of peak power are in the 20 to 40 mg/kW range, turning catalyst cost tolerable even noble metals are used.

5 CONCLUSIONS

This paper showed that tubular geometries with porous wall micrometer diameter tubes and nanometer pores scales in wall material have very good current and reactants transport characteristics that allow high efficiency in catalyst use. All parts were produced individually in small amounts with till now unstable processes, described in section 3, in laboratories with very few resources, and this creates the hope that with proper funding this kind of cell becomes a reality in a reasonable time. Numerical simulation showed peak power till 48kW/dm^3. The results are suitable for transportation usage besides low catalyst cost. The low transport phenomena of the design also turn it promising the use of non-Pt catalysts. Other interesting point is that anode hydrogen permeable metal thin shells in each μm tube, allows direct H$_2$ filtering, easing reformer task, and protecting fuel tank to O$_2$ contamination.

6. REFERENCES

Al-Baghdadi, M.A.R.S., 2005, "Modeling of proton exchange membrane fuel cell performance based on semi-empirical equations", Renewable Energy, Vol. 30, pp. 1587-1599.

Antoine,O., Bultel, Y.and Durand, R., 2001, "Oxygen reduction reaction kinetics and mechanism on platinum nanoparticles inside Nafion", Journal of Electroanalytical Chemistry, Vol. 499, pp. 85-94

Antunes, E.F., Lobo, A.O., Corat, E.J., Trava-Airoldi,V.J., Martin, A..A.. and Veríssimo, C., 2006, "Comparative study of 1st and 2nd order Raman spectra of MWCNT at visible and infrared laser excitation", Carbon, Vol. 44, pp. 2202-2211.

Bambace, L.A.W., Ramos, F.M., Villanova, H.F., Castro, A.J.A. and Favalli, R.C., 2007, "New fuel cell architectures and the role of electrokinetic flows in its performance", Proceedings of VII Congresso Latino Americano de Geração e Transmissão de Energia Elétrica, Vol.1, Vinã del Mar, Chile, pp 1-8

Bambace, L.A.W., Castro, A.J.A., ,Favalli, R.C., Ramos, F. and Villanova, H.F., 2008, "Tubular Anodes with Hidden Catalyst Concept and their Hydrogen Transport", Proceedings of WREC X World Renewable Energy Congress, Vol.1, Glasgow. Scotland.

Bennett, P., 2006., "GEO 387E-Environmental Organic Geochemistry Lecture Notes: VI Sorption.", On line course. Texas University. http://www.geo.utexas.edu/courses/387e/PDF/sorption.pdf.

Bizzotto, D., 2002, "Chemistry 517 Interfacial Electrochemistry", On-line Course. University of British Columbia. http://www.chem.ubc.ca/faculty/bizzotto/chem517/chem517_intro.pdf.

Brady M.P., Weisbrod, K., Paulauskas, I., Buchanan, R.A., More K.L., Wang, H., Wilson, M., Garzon, F. and Walker, L.R., 2004, "Protection of Metallic Bipolar Plates in PEM Fuel Cells", Scripta Materialia, Vol. 50, pp. 1017-1022.

Chang,H., Joo, SH. and Pak, C., 2007, "Synthesis and characterization of mesoporous carbon for fuel cell applications", J. Mater. Chem., Vol. 17, pp. 3078-3088.

Cheek, H.C., Long, H.C. and Trulove, P.C., 1999, "Electrodeposition of Niobium and Tantalum from a room temperature molten salt system", Proceedings of International Symposium (12th) on Molten Salts and the 1999 Joint International Meeting, Vol. 1, Honolulu, Hawaii.

Corry, B., Kuyucak,S. and Chungy, S., 2003, "Dielectric Self-Energy in Poisson-Boltzmann and Poisson-Nernst-Planck Models of Ion Channels", Biophysical Journal, Vol. 84, pp. 3594-3606.

Dadzie, S.K. and Méolans, J. G., 2005, "Temperature jump and slip velocity calculations from an anisotropic scattering kernel", Physica A, Vol. 358, pp. 328-346.

Ledoux, M.J., Gulino, G., Vieira R., Amadoua, J., Nguyena, P., Galvagno, S., Centi. G. and Pham-Huua, C., 2004, "Composites based on carbon nanotubes or nanofibers deposited on an activated support for use in catalysis", EP1448477.

Ledoux, M.J., Gulino,G; Vieira R., Amadoua, J., Nguyena, P., Galvagno, S., Centi, G. and Pham-Huua,C., 2005, "C_2H_6 as an active carbon source for a large scale synthesis of carbon nanotubes by chemical vapour deposition", Applied Catalysis A: General, Vol. 279, pp. 89-97.

Mitchel, W., 1963, "Fuel Cells", Academic Press,. London., 428 p..

Ramos, E., Juarez, H., Flores, C., 2008, "Fuel Cells: Navier-Stokes and Poisson–Nernst–Planck equation", Proceedings of I Workshop on Asymptotics for Parabolic and Hyperbolic Systems – LNCC, Vol. 1, Rio de Janeiro, Brasil, pp. 1-25.

Roshandela,R., Farhanieha, B.and Saievar-Iranizadb, E., 2005, "The effects of porosity distribution variation on PEM fuel cell performance", Renewable Energy, Vol. 30, pp. 1557-1572.

Silva, DF., Spinace, E.V., Oliveira Neto, A., Pino, E.S. and Cruz, V.A., 2005, "Processo de preparação de eletrocatalisadores utilizando processos radiolíticos para aplicação em células a combustível com membrana trocadora de prótons", PI0505416-8.

Sun,H., Liu,H., and Guo,L.J., 2005, "PEM fuel cell performance and its two-phase mass transport", Journal of Power Sources, Vol. 143, pp. 125-135.

Swartzentruber, B. S., 1996, "Direct Measurement of Surface Diffusion Using Atom-Tracking Scanning Tunneling Microscopy", Phys. Rev. Lett., Vol. 76, pp. 459-462.

Tennison, S.R. and Sowerby, B., 2003, "Fuel cell structure", EP1316120.

Thampan, T., Malhotra, S., Zhang, J., and Datta, R., 2001, "PEM fuel cell as a membrane reactor", Catalysis Today, Vol. 67, pp. 15-32.

Vermilyea, D.A., 1957, "Electrodeposition on Metal Whiskers", The Journal of Chemical Physics, Vol. 27, pp. 814-815.

Xue, Y., 2007, "Experimental study of electrical conductivity of carbon nanotube, nanofiber buckypapers and their composites, MSc Thesis. Florida State University".

7. RESPONSIBILITY NOTICE

The authors are the only responsible for the printed material included in this paper.